Vertical GaN nanocolumns grown on graphene intermediated with a thin AlN buffer layer

Andreas Liudi Mulyo[1,2], Mohana Krishnappa Rajpalke[1,a)], Haruhiko Kuroe[2], Per-Erik Vullum[3], Helge Weman[1], Bjørn-Ove Fimland[1,b)] and Katsumi Kishino[2,4,b)]

[1] Department of Electronic Systems, Norwegian University of Science and Technology (NTNU), NO-7491 Trondheim, Norway

[2] Department of Engineering and Applied Sciences, Sophia University, 102-8554, Tokyo, Japan

[3] SINTEF Industry, NO-7465 Trondheim, Norway

[4] Sophia Nanotechnology Research Center, Sophia University, 102-8554, Tokyo, Japan

[a)] Present address: Center for Quantum Devices, Niels Bohr Institute, University of Copenhagen, 2100 Copenhagen, Denmark

[b)] E-mail: bjorn.fimland@ntnu.no and kishino@sophia.ac.jp

Abstract

We report on the self-assembled growth of high-density and vertically-oriented *n*-doped GaN nanocolumns on graphene by radio-frequency plasma-assisted molecular beam epitaxy. Graphene was transferred to silica glass, which was used as substrate carrier. Using a migration enhanced epitaxy grown AlN buffer layer for the nucleation is found to enable a high density of vertical GaN nanocolumns with *c*-axis growth orientation on graphene. Furthermore, micro-Raman spectroscopy indicates that the AlN buffer reduces damage on the graphene caused by impinging active N species generated by the radio-frequency plasma source during the initial growth stage and nucleation of GaN. In addition, the grown GaN nanocolumns on graphene are found to be virtually stress-free. Micro-photoluminescence measurements show near band-edge emission from wurtzite GaN, exhibiting higher GaN bandgap related photoluminescence intensity relative to a reference GaN bulk substrate and the absence of both yellow luminescence and excitonic defect emission. Transmission electron microscopy reveals the interface of GaN nanocolumns on graphene via thin AlN buffer layer. Even though the first few monolayers of AlN on top of graphene are strained due to in-plane lattice mismatch between AlN and graphene, the grown GaN nanocolumns have wurtzite crystal structure without observable defects. The results of this initial work pave the way towards realizing low-cost and high-performance electronic and optoelectronic devices based on III-N semiconductors grown on graphene.

1. Introduction

For the past two decades, the III-N system has met its high expectations as one of the most promising wide band-gap semiconductors materials for visible, violet and ultraviolet light emitting devices (LEDs) [1-3] and high-power electronics [1, 4]. The most commonly used substrates today for III-N materials are Si, SiC and Al_2O_3 [5]. However, these substrates have inadequate compatibility with the III-N system as they are characterized by large lattice constant mismatch, large thermal coefficient mismatch, poor thermal conductivity, low thermal stability and/or non-transparent substrate [5]. These issues may be overcome by utilizing graphene [6-9] as a substrate for the epitaxial growth of III-N. In addition, graphene offers an excellent electrical conductivity [10] and thus potentially can become a combined substrate and transparent electrode for improving the performance and functionalities of III-N-based optoelectronic devices. However, the absence of dangling bonds for graphene causes high surface tension, leading to weak nucleation and cluster growth [6, 11] which likely generate high-density of stacking faults [11, 12] or threading dislocations [13] when GaN thin-film structures are grown on it.

By exploiting the defect-suppressing property of nanowire or nanocolumn structures [14-16], there is a likelihood to overcome these limitations in order to realize high quality GaN on graphene. Additionally, their geometry can provide enhanced light extraction efficiency which is beneficial for LEDs [17]. Number of works have reported the growth of GaN nanocolumns on graphite [18], epitaxial graphene on SiC [19], transferred graphene and multi-layer graphene on various substrate carriers [20-25] such as Si, SiO_2 and Al_2O_3. However, it is generally observed that the grown GaN nanocolumns on graphene have either low density [22-24] or are oriented in non-defined directions [20], which are not desirable for light emitter applications as this can reduce light extraction and emission efficiency. Despite that preferred characteristics of GaN nanowires grown directly on graphene were obtained by Kumaresan *et al.* [21], the graphene's properties after the GaN growth were not evaluated. This issue was addressed by Fernández-Garrido *et al.* [19] remarking the complete graphene removal after GaN nanowire growth. These findings discourage the graphene's prospective as an integrated part of GaN-based devices as a combined substrate and transparent electrode. Growth of high density and vertically aligned GaN nanocolumns on multi-layer graphene (~35 nm thick) were successfully demonstrated by Hayashi *et al.* [25]. However, due to the thickness of the multi-layer graphene, it is highly absorbing and cannot be used as a transparent electrode.

Here, we present the growth, structural and optical characterization of GaN nanocolumns grown on transferred (single-layer) graphene on silica glass by radio-frequency plasma-assisted molecular beam epitaxy (RF-PAMBE) utilizing a thin AlN buffer layer. The morphology of the grown GaN nanocolumns was investigated via scanning electron microscopy (SEM). The structural properties of GaN nanocolumns and graphene were analyzed by micro-Raman spectroscopy. The optical quality of the grown GaN nanocolumns was studied by micro-photoluminescence at room temperature (RT). Later, the sample with the optimized growth condition of GaN nanocolumns on graphene is further characterized using transmission electron microscopy (TEM) to examine the structure and chemistry of the grown GaN nanocolumns. We demonstrate the growth of high-density, vertically-aligned and high-quality single crystalline wurtzite (hexagonal) GaN nanocolumns on graphene intermediated with a thin AlN buffer layer. There is a strong impact from the AlN buffer layer, as it serves not only as nucleation sites for the GaN nanocolumn growth, but also alleviates damage of the graphene.

2. Experimental methods

The substrate was commercially available graphene grown by chemical vapor deposition (CVD) on Cu foil [26] and transferred onto silica glass which was used as the substrate carrier. It should be pointed out that the graphene used in this work refers to the mono (single-) layer of sp^2-bonded carbon atoms tightly packed into a hexagonal two-dimensional lattice, with a theoretical thickness of approximately 0.335 nm. Silica glass was chosen not only because it is cheap, but also due to its excellent optical transparency in the visible and ultraviolet region, which might be useful for flip-chip III-N based LEDs fabrication. In the following, all the values of substrate temperature were based on pyrometer reading. Sample 1 was *n*-type (Si) doped GaN nanocolumns grown directly on graphene at a substrate temperature of 895 °C for 90 min, using the established growth condition for GaN nanocolumns on silica glass, as described in our previous work [14]. For sample 2, the *n*-GaN nanocolumns were synthesized identical to sample 1, but with GaN as a buffer layer. This particular buffer layer was formed at a substrate temperature of 690 °C. Ga atoms were first continuously deposited on the graphene for 35 s and then nitrided with N_2 plasma for 60 s. In the case of sample 3, AlN was used as a buffer layer for the *n*-GaN nanocolumns instead of GaN. This layer was deposited at a substrate temperature of 805 °C using migration-enhanced epitaxy (MEE) [27, 28] with alternating supplies of Al atoms and N_2 plasma in a 20-period cycle consisting of: Al supply (4

s), interrupt (5 s), and N_2 plasma (3 s) [25]. Subsequently, GaN nanocolumns were grown under the same conditions as for sample 1.

SEM images were acquired using an SII SMI3050SE focused ion beam-SEM (FIB-SEM) and a Hitachi SU8000 SEM at respective acceleration voltages of 15 kV and 10 kV. Unpolarized Raman spectra were measured at RT in backscattered configuration using a Renishaw InVia Reflex Spectrometer System equipped with a 514.5 nm excitation laser. The laser was focused onto the sample using a 100× objective lens resulting in a spot diameter of ~1.5 μm, and the scattered Raman signal was collected by the same objective lens. Micro-photoluminescence was carried out at RT using a HeCd laser (325 nm) as the excitation source where a 100× objective lens was used to focus the laser beam (spot diameter of ~2 μm) and for the collection of the scattered light. Finally, the TEM analysis was performed with a double Cs corrected cold field emission gun JEOL ARM200F, operated at 200 kV. The TEM images were taken with the nanocolumns oriented along the [1-210] zone axis. The cross-section TEM specimen was prepared with a FEI Helios G4 UX FIB-SEM. Coarse thinning was performed at 30 kV acceleration voltage, while the final thinning was performed at 5 kV and finally 2 kV to minimize surface ion-beam damage.

3. Results and discussion

SEM images of samples 1, 2 and 3 are presented in Figure 1. The grown GaN nanocolumns in sample 1 (Figure 1(a) and (b) for bird- and side-view SEM, respectively) are characterized with random growth directions, and exhibit irregular diameters and heights (Figure 1(b)). Additionally, the formation of GaN islands are observed (red-circled in Figure 1(b)), which might be a result of the high surface tension (low surface energy) caused by the chemical inertness of graphene [6, 11]. Furthermore, irradiation of N_2 plasma at the initial growth stage may generate defects in graphene [29-31] or even decompose it [32].

One approach in preventing the direct N_2 plasma on graphene could be to cover the surface area of graphene with continuous Ga atom deposition at low substrate temperature before it is subjected to nitridation to form a GaN buffer layer. For GaN nanocolumn growth on Si(111) [33] it has been shown that this method leads to a high density of dot-like GaN nucleation layers, rather than a thin film, which is crucial to maintain the formation of nanocolumns. In addition, such low temperature (e.g. 690 °C) is expected to reduce graphene's reactivity with the incoming N atoms, thus decreasing the graphene damage upon nitridation, as was the case for

a graphene oxidation process [34]. As shown in Figure 1(c) and (d) for the bird- and side-view SEM, respectively, the density, diameter uniformity and verticality of the GaN nanocolumns show an improvement compared to sample 1, although they have a tendency to grow in non-perpendicular directions relative to the substrate. Nevertheless, one should consider that the epitaxy of GaN on graphene can partially break the C-C σ bonds of graphene upon expansion of the graphene lattice, where the interface strain is reduced significantly by chemical bonding between C and N atoms, as suggested by Gohda and Tsuneyuki [35]. Compared to samples 1 and 3, sample 2 has the highest vertical nanocolumn length (1750 nm). Additionally, it is noticed from the top facet that the nanocolumns in sample 2 are likely Ga-polar (pyramidal tips [36, 37]), whereas samples 1 and 3 are N-polar (flat tips [36, 37]), as shown in Figure 1(d), (b) and (f), respectively.

To reduce the graphene damage from direct bombardment of active N atoms and alleviate in-plane strain caused by GaN nucleation, an AlN buffer layer was deposited using MEE technique on the graphene surface prior to GaN nanocolumn growth. The MEE technique enhances the surface migration of Al atoms [38], increasing their coverage area on graphene in the absence of N atoms. Due to the polycrystalline nature of CVD grown graphene [39] and its extremely low surface energy [11], AlN tends to form islands [25] instead of a thin-film. Nonetheless, AlN has greater likelihood than GaN to nucleate on graphene via *quasi*-van der Waals forces due to the higher adsorption energy of Al [40] and stronger bonding of Al-N relative to Ga-N [35, 41], Moreover, the graphene lattice is expected to be preserved for AlN grown on graphene due to that the in-plane strain is not large enough to induce structural deformation of the graphene [35]. This is corroborated by the observation of Al Balushi *et al.* [42], where nucleated polycrystalline islands of AlN (grown by metalorganic CVD) on epitaxial graphene did not significantly distort the underlying graphene. We observe that the presence of the AlN buffer layer in sample 3 promotes the perpendicular growth orientation and increases the density of GaN nanocolumns on graphene (Figure 1(e) and (f) for bird- and side-view SEM, respectively). The role of the AlN buffer layer as nucleation site leads to a quite uniform morphology of vertically aligned GaN nanocolumns (Figure 1(f)) with an average diameter, height and density of 90 nm, 1015 nm and 1.5×10^9 cm^{-2}, respectively. As a note, we manage to obtain almost twice as high density as that of the work of Hayashi *et al.* [25] using the same MEE growth conditions in which multi-layer graphene was employed as the substrate for GaN nanocolumn growth. Having a denser nanocolumn density is more beneficial in further device processing for the fabrication of e.g. nanocolumn-based ultraviolet LEDs, i.e. preventing the

usage of a polyimide insulating layer which can degrade light extraction efficiency due to the ultraviolet light absorption by the polyimide.

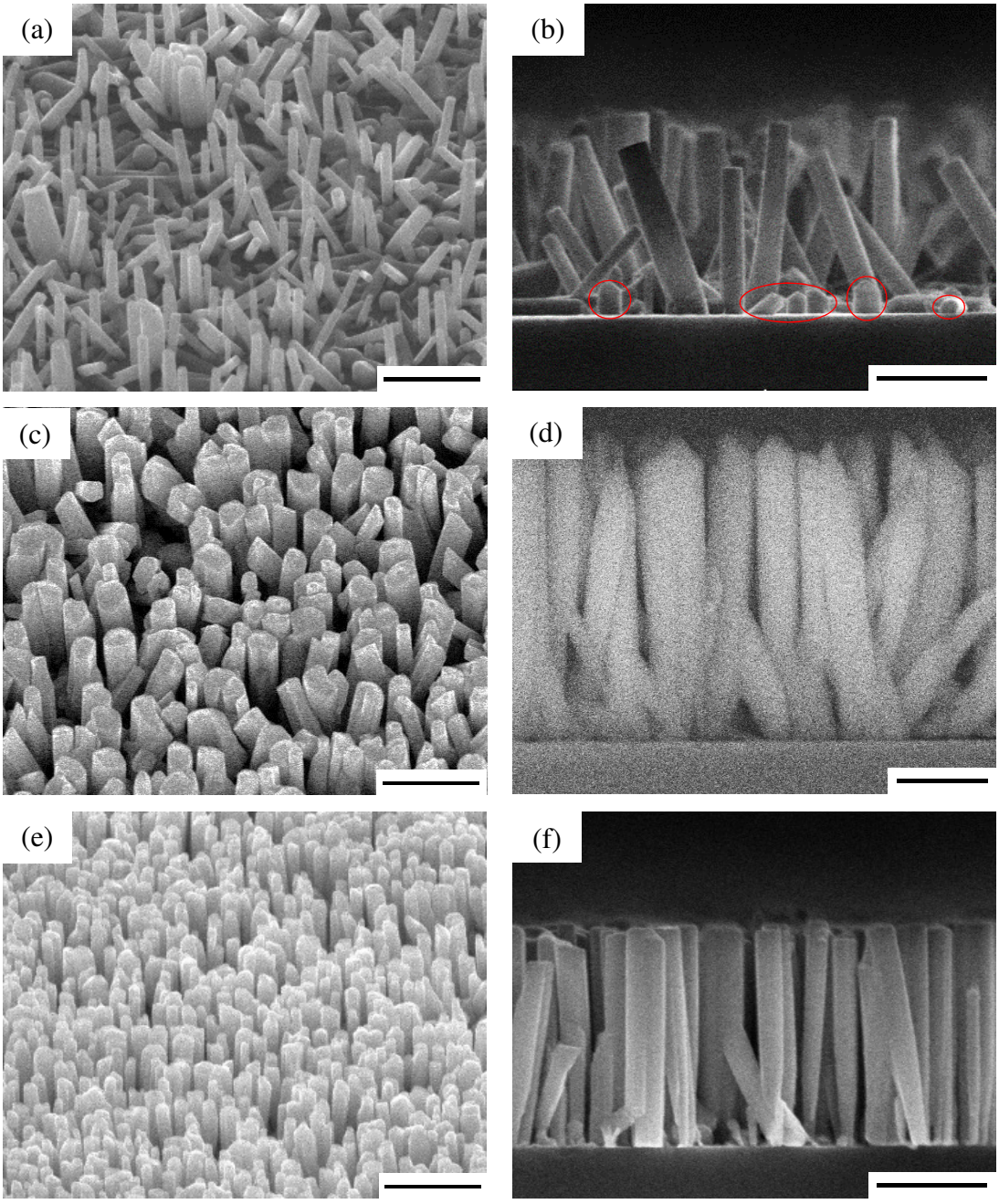

Figure 1. (a, b), (c, d) and (e, f) are (bird-, side-) view SEM images of samples 1, 2 and 3, respectively. Red circles in Figure 1(b) indicate the formation of GaN islands. Scale bars are 1 μm for (a, c and e) while 500 nm for (b, d and f).

Structural properties of the nanocolumn samples were further characterized using micro-Raman spectroscopy in the range between 500 and 800 cm^{-1}, where the spectra are shown in Figure 2(a). Regardless of the growth conditions, all of these nanocolumn samples have the

same wave number for the A_1 (TO), E_1 (TO) and E_2 (high) phonon modes at 531.9, 557.3 and 566.2 cm^{-1}, respectively, all of which are typical values for GaN with a wurtzite crystal structure [43]. These observations are similar to that of self-organized GaN nanocolumns grown on Al_2O_3 and Si substrates [44], as well as to that of regularly arrayed GaN nanostructures [45]. Notably, there is no sign of any TO phonon mode at 554 [46] or 555 cm^{-1} [43], suggesting that there is no existence of zinc blende (cubic) GaN in the nanocolumn samples. Moreover, the Raman shift for the obtained E_2 (high) mode is consistent with the reported value for homoepitaxially grown GaN films at a phonon frequency of 566.2 cm^{-1} [47], demonstrating that the GaN nanocolumns in samples 1, 2 and 3 can be considered to be stress-free. In this work, we could not observe an A_1 (LO) phonon mode which is normally detected at 737 cm^{-1} [43-45]. It could be that its weak intensity [44] is overlapped with the broad signal ranging from ~650 to ~750 cm^{-1}. This broad signal might be affiliated to the Fröhlich mode, which is a surface-related vibrational mode [44, 45]. Expected Raman-active phonon modes for AlN in sample 3, for instance A_1 (TO) at 614 cm^{-1}, E_2 (high) at 660 cm^{-1} and E_1 (TO) at 673 cm^{-1} [48], are not observed, which could be due to the small excitation volume of the AlN nucleation layer.

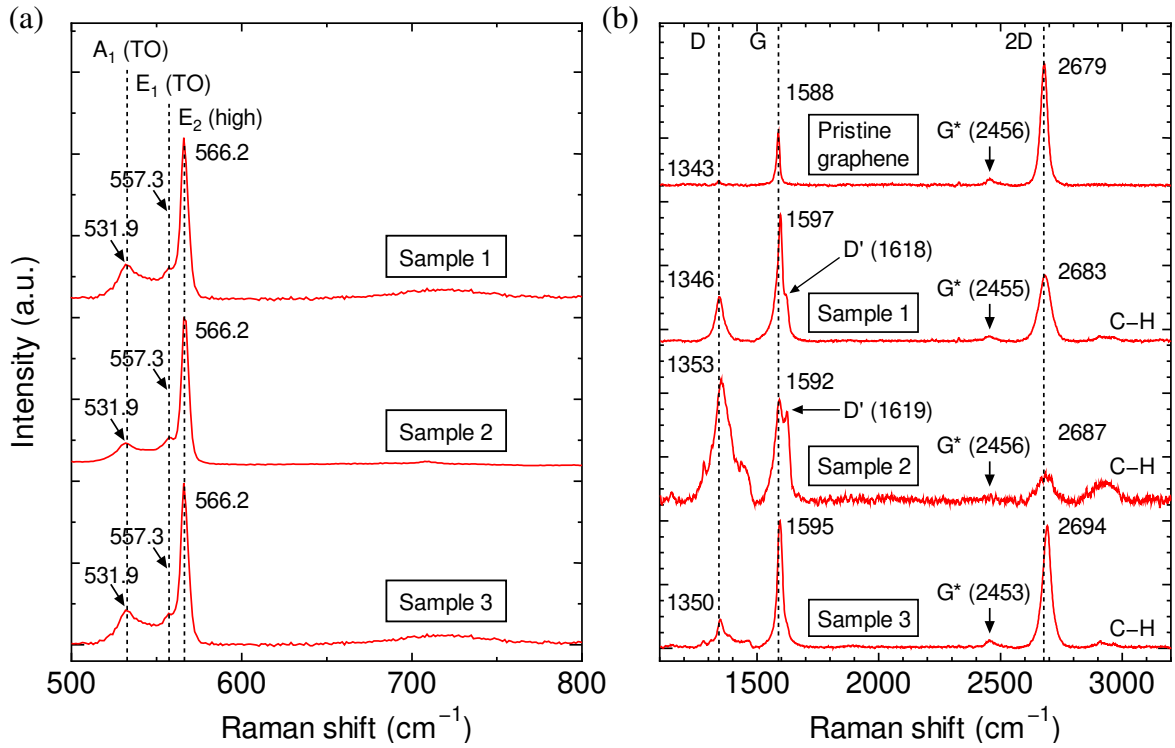

Figure 2. Micro-Raman spectra of (a) samples 1, 2 and 3 between 500 and 800 cm^{-1} and of (b) pristine graphene and samples 1, 2 and 3 between 1100 and 3200 cm^{-1}. The dashed lines in (b) indicate the D, G and 2D peak positions of pristine graphene.

To identify the damage of graphene in samples 1, 2 and 3, micro-Raman measurements from 1100 to 3200 cm^{-1} (Figure 2(b)) were carried out with pristine graphene transferred onto silica glass as the reference sample. This characterization technique gives rise to well-established first- and second-order Raman scattering mechanisms in undoped graphene [49]. Although graphene is only consisted of one atomic layer of carbon sheet, it exhibits very strong Raman scattering due to the double resonance mechanism in graphene. The first-order Raman band, known as the G band (1588 cm^{-1}), is a doubly degenerate (in-plane transverse optical (iTO) and longitudinal optical (LO)) phonon mode at the Brillouin zone center. On the other hand, the second-order Raman process involves an intervalley double resonance scattering of two iTO phonons near the K point of the Brillouin zone (2D band at 2679 cm^{-1}), and also an intervalley double resonance scattering of one iTO phonon with one defect mode near the K point of the Brillouin zone (D band at 1343 cm^{-1}). A subtle D peak with prominent G and 2D peaks where the intensity ratios of $I_D/I_G \approx 0$ and $I_{2D}/I_G \approx 2$, indicate the high quality of pristine graphene used for the growths reported in this paper. After the GaN nanocolumn growth, sample 1 and moreover sample 2 clearly show higher I_D/I_G and lower I_{2D}/I_G ratios compared to sample 3, implying that the direct exposure of N_2 plasma and GaN nucleation on graphene contribute to a higher degree of damage relative to the graphene which is covered with an AlN buffer layer. In addition, sample 1 exhibits a D′ peak in the Raman spectrum (more prominent for sample 2), which is described as a disorder-induced feature in the graphene crystalline lattice [49]. The aggravated graphene damage in sample 2 is possibly caused by the sole irradiation of N_2 plasma following the deposition of Ga atoms on the graphene surface, together with the in-plane strain generated by the subsequent formation of GaN nucleation [42].

Also, the N_2 plasma treatment can modify the chemical properties and electronic structure of graphene, where N atoms form a covalent bonding with C atoms and change the lattice structure of graphene [29, 50]. There are mainly three probable bonding configurations for the incorporated N atoms in the graphene network (pyridinic N, pyrrolic N and graphitic N), all of which can influence the electrical properties of graphene [30, 31, 50-52]. Earlier works have shown that N-doping of graphene by NH_3 plasma [29, 30] or N_2 plasma [31] results in *n*-type doping, where the Fermi level is shifted above the Dirac point [53] and the work function becomes smaller than the reported value of undoped graphene [31, 51]. Please note that the nitrogen doping in graphene is likely to be inhomogeneous. In the Raman mapping analysis on N-doped graphene performed by Luo *et al.* [54], it was revealed that some spots have high I_D/I_G ratio and some show very low I_D/I_G ratio, which suggests a non-uniform defect distribution

induced by inhomogeneous nitrogen incorporation in the graphene. According to the results shown in Figure 2(b), the most prominent features in the micro-Raman spectra of graphene (G and 2D bands) in samples 1, 2 and 3, as well as the defect-related D band, are generally shifted to higher wavenumbers relative to the pristine graphene. The blue-shift of the D and G peak can be explained by local electron/hole doping in carbon nanostructures [30, 55-57], while the blue-shift of the 2D peak can be the result of doping and/or compressive strain [56, 57]. Based on these observations, it is plausible that the nitrogen-treated graphene presented in this paper exhibits an *n*-type semiconductor behavior. To precisely determine the nitrogen content as well as identify the bonding configurations of N atoms in the graphene samples presented in this paper, future studies employing X-ray photoelectron spectroscopy and/or ultraviolet photoelectron spectroscopy measurements are necessary. Apart from the aforementioned peaks, the adsorption of hydrocarbon (C-H) is detected after GaN growth, which is consistent with the work reported by Fernández-Garrido *et al.* [19] It is also noted that the existence of a G* peak, which originates from the overtone modes (transition from the ground state to the second or higher excited state) of a second-order Raman process involving an intervalley double resonance scattering of two LO phonons near the K point of the Brillouin zone [58], is fairly observable in the pristine graphene, samples 1 and 3, whereas its presence is rather faint for sample 2. Despite being exposed to different growth conditions, the position of the G* peak is relatively stable compared to the earlier discussed D, G and 2D peak positions. Further studies are required to clarify these phenomena, which are beyond the focus of this paper.

Evaluation of the optical properties of samples 1, 2 and 3 was done via micro-photoluminescence at RT using a He-Cd laser (325 nm) as excitation source. A freestanding hydride vapor phase epitaxy (HVPE)-grown GaN bulk substrate with a threading dislocation density of 6-8 × 10^6 cm^{-2} was used as a reference, like for previous studies [14-16, 25]. Photoluminescence spectra of sample 1 (blue line), sample 2 (green line), sample 3 (red line), and the reference sample (black line) are presented in Figure 3. Here, it is established that there are strong luminescence from GaN in samples 1, 2, 3 and reference sample, whose peak wavelengths are located at 364.6, 364.3, 364.6 and 363.6 nm, respectively. Although a red-shift of 0.7 to 1.0 nm relative to that of the reference sample is shown by the nanocolumn samples, the observed excitonic emission of near 364 nm can still be related to the wurtzite GaN bandgap. The linewidths in samples 1 and 3 are slightly narrower (full-width at half-maximum (FWHM) of 8.69 and 9.14 nm, respectively) than the reference sample (FWHM of 10.79 nm), whereas

for sample 2 it is somewhat wider (FWHM of 11.77 nm). In general, there are not much striking differences in the linewidth between the nanocolumn samples and the reference sample.

It is also noticeable that all of the nanocolumn samples exhibit higher GaN band-edge photoluminescence peak intensity as compared to the reference sample, where the intensity is ~1.9 times higher for sample 1, ~1.2 times higher for sample 2 and ~2.3 times higher for sample 3. Interestingly, GaN nanocolumns in sample 1, which exhibit rather random (non-vertical) growth orientations (Figure 1(a) and (b)), demonstrate much higher photoluminescence intensity as compared to GaN nanocolumns in sample 2, where the growth orientation is more defined in terms of verticality (Figure 1(c) and (d)). The low photoluminescence intensity could be due to the fact that the lower part of many nanocolumns in sample 2 are coalesced with each other, as can be clearly seen from Figure 1(d). On the other hand, the intensity ratio shown by sample 3 should be highlighted, as the optical quality of this sample is similar with that of the GaN nanocolumns grown on other types of substrates, for instance silica glass [14], multi-layer graphene [25] and selective area growth on sputtered AlN/Si(111) where the diameter of nanocolumn is 200 nm [16] (such comparison is valid here since the same reference sample has also been used for other papers [14-16, 25]). Unlike sample 2, the base part of the GaN nanocolumns in sample 3 is less likely to show any coalescence, as shown in Figure 1(f).

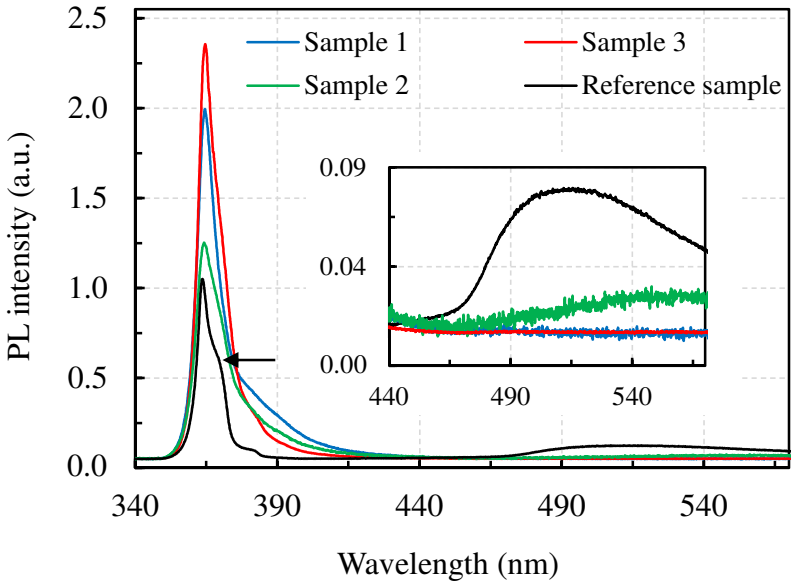

Figure 3. Photoluminescence spectra of samples 1 (blue line), 2 (green line) and 3 (red line) and a reference GaN bulk sample (black line) measured at RT. Inset shows magnified spectra from

440 to 580 nm. The black arrow pointing to the spectrum of the reference sample highlights the shoulder peak observed at 369 nm related to excitons bound to structural defects [59].

Furthermore, there are some noteworthy differences in the photoluminescence spectra from the nanocolumn and reference samples that should be mentioned here. First, nanocolumn samples do not exhibit a shoulder peak at 369 nm, which is affiliated with excitons bound to structural defects [59], unlike what is observed in the reference sample (indicated with the black arrow in Figure 3). A second distinct difference is the presence of a yellow luminescence band, which is solely observed in the reference sample. In general, all of the nanocolumn samples indicate a strong suppression of this broad emission in the wavelength range from 465 to 570 nm (a magnified spectrum of this yellow luminescence band is shown in the inset of Figure 3). For GaN nanocolumns in samples 1 and 3, it is clearly observed that this yellow band is completely eliminated, which indicates that there are no electron transitions from the conduction band to the deep acceptor levels [60, 61]. However, a small deviation from this is shown in sample 2, which exhibits a weak emission in the proximity of the yellow luminescence band. Zinc blende GaN-related emission, which typically occurs at ~386 nm [12], is not observed for any of the samples.

According to the SEM, micro-Raman spectroscopy and micro-photoluminescence results on three different growth conditions of GaN nanocolumns on graphene, it is clear that sample 3 represents the best sample. The superior properties of sample 3, being vertically grown GaN nanocolumns exhibiting high photoluminescence peak intensity and reduced graphene damage, are promising for the envisaged nanocolumn/graphene-based devices. For these reasons, further characterizations by TEM were carried out solely based on sample 3.

A cross-section bright field TEM (BF TEM) image (sample 3) from a region covering the top of the silica glass, the graphene, the AlN buffer layer, and the bottom of the GaN nanocolumn is shown in Figure 4(a). The graphene layer is observed on top of the silica glass substrate (blue arrows) and interestingly, the contrast from graphene disappears at a few locations (indicated by red arrows). It has been observed that the graphene layer is continuous without any holes in it, as the wrinkles associated with the thermal expansion coefficient difference between Cu and graphene during the synthesis are also found to cross Cu grain boundaries [26]. However, it buckles and bends. The lack of contrast from graphene is likely due to local bending (since silica glass surface is not atomically flat) that makes the graphene deviate from edge-on orientation, and hence the lattice contrast disappears from the TEM image.

Since all TEM images are projections that average through the thickness of the TEM lamella, local steps or height variations on the silica surface can possibly make a single-layer graphene appear as two or three layers in the TEM images. Similarly, TEM images of the transferred graphene on Si in the work of Heilmann *et al.* [24] show how the graphene is not flat, due to unavoidable formation of amorphous SiO_x layer. In contrast, imaging epitaxial graphene, for example on atomically flat SiC single crystals, results in an unambiguous visualization of the number of graphene layers [6, 19, 42].

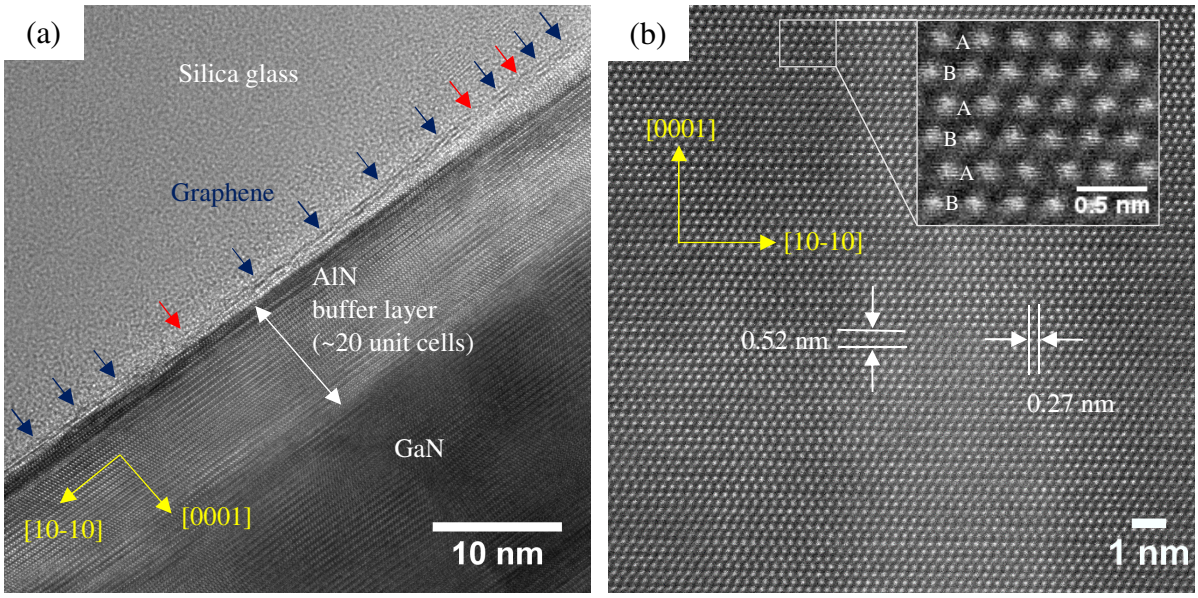

Figure 4. TEM images of sample 3 taken along the [1-210] zone axis. (a) BF TEM image of the interfaces between GaN nanocolumn, AlN buffer layer, graphene and silica glass. The blue arrows point to sites where the presence of graphene is clearly seen in the image, whereas the red arrows point to sites where the presence of graphene is not revealed, probably due to local bending of graphene at those specific sites causing a lack of lattice contrast. (b) High resolution HAADF STEM image from the middle of the GaN nanocolumn (inset: crystal stacking order of wurtzite GaN).

The AlN buffer layer grown on the graphene is found to be of pure wurtzite crystal structure and can be seen in Figure 4(a) as an ~20 unit cells (~10 nm) thick layer with predominantly bright contrast. The dark contrast at the bottom (next to the graphene) most likely represents strain contrast due to the in-plane lattice mismatch between AlN and graphene. This strain contrast is only present in the first few monolayers of AlN. However, it is noticed that the strain contrast is not uniform along the interface between AlN and graphene. There are both dark and

bright regions close to the graphene interface. The primary reason for this is that the strain is actually inhomogeneously distributed. When dislocations are present, the strain will always vary in the vicinity of a dislocation, i.e. atoms and planes are differently distorted (displaced away from their bulk equilibrium positions) according to the position of the dislocation. The same is also true for point like lattice defects. Nevertheless, no indication of defect propagations, such as stacking faults or threading dislocations, is observed in the GaN nanocolumn (dark contrast) grown on this AlN buffer layer.

High resolution high-angle annular dark field scanning TEM (HAADF STEM) image from the middle of the nanocolumn (Figure 4(b)) shows clearly the Ga atomic columns (represented by white dots) which have an *ABAB* stacking order (see inset of Figure 4(b) for easier observation). The interplanar spacings of GaN nanocolumns parallel to the [0001] and [10-10] directions, deduced from the image presented in Figure 4(b), are approximately 0.52 and 0.27 nm, respectively, in good agreement with the established lattice constant parameters for GaN [5, 14, 25]. This STEM image demonstrates single crystalline GaN with a perfect wurtzite structure without any observable defects or inversion domain boundaries in the field of view.

4. Conclusion

In summary, we have demonstrated that growth of high-density and vertically-aligned GaN nanocolumns on graphene/silica glass by RF-PAMBE is feasible using a thin AlN buffer layer. The AlN, grown using MEE technique, does not only serve as nucleation sites for the GaN nanocolumns, but it also provides considerable protection to the graphene from the N_2 plasma source and in-plane strain generated by GaN nucleation. It is proven that when using an AlN buffer layer, the stress-free GaN nanocolumns are grown in the *c*-axis direction with wurtzite structure and exhibit an acceptable verticality. Furthermore, the columnar structure of GaN provides higher photoluminescence intensity and higher structural quality than that of a reference HVPE-grown GaN bulk substrate. TEM of representative GaN nanocolumns demonstrates a high-quality wurtzite crystal structure with the absence of threading dislocations, stacking faults or twinning defects. These findings are therefore very encouraging for further establishing graphene as an alternative substrate to enhance the performance and functionalities of III-N-based semiconductor devices in general.

Acknowledgements

We thank Y. Konno, I. M. Høiaas, D. Ren and A. T. J. v. Helvoort for fruitful discussions. We are also indebted to K. Yamano and I. Matsuyama for dedicated MBE maintenance. This work was supported by the NANO2021 (Grant No. 259553) program of the Research Council of Norway and by Japan Society for the Promotion of Science KAKENHI (Grant No. 24000013). The Research Council of Norway is also acknowledged for the support to NTNU NanoLab through the Norwegian Micro- and Nano-Fabrication Facility and to the Norwegian PhD Network on Nanotechnology for Microsystems (FORSKERSKOLER-221860). The TEM work was carried out on the NORTEM infrastructure (Grant No. 197405) TEM Gemini Centre, NTNU.

References

[1] Shizuo F 2015 Wide-bandgap semiconductor materials: For their full bloom *Jpn. J. Appl. Phys.* **54** 030101
[2] Kishino K, Yanagihara A, Ikeda K and Yamano K 2015 Monolithic integration of four-colour InGaN-based nanocolumn LEDs *Electron. Lett.* **51** 852-4
[3] Yamano K and Kishino K 2018 Selective area growth of InGaN-based nanocolumn LED crystals on AlN/Si substrates useful for integrated μ-LED fabrication *Appl. Phys. Lett.* **112** 091105
[4] Kuzuhara M, Asubar J, T. and Tokuda H 2016 AlGaN/GaN high-electron-mobility transistor technology for high-voltage and low-on-resistance operation *Jpn. J. Appl. Phys.* **55** 070101
[5] Guoqiang L, Wenliang W, Weijia Y, Yunhao L, Haiyan W, Zhiting L and Shizhong Z 2016 GaN-based light-emitting diodes on various substrates: a critical review *Rep. Prog. Phys.* **79** 056501
[6] Munshi A M, Dheeraj D L, Fauske V T, Kim D-C, van Helvoort A T J, Fimland B-O and Weman H 2012 Vertically Aligned GaAs Nanowires on Graphite and Few-Layer Graphene: Generic Model and Epitaxial Growth *Nano Letters* **12** 4570-6
[7] Seol J H, Jo I, Moore A L, Lindsay L, Aitken Z H, Pettes M T, Li X, Yao Z, Huang R, Broido D, Mingo N, Ruoff R S and Shi L 2010 Two-Dimensional Phonon Transport in Supported Graphene *Science* **328** 213
[8] Kim K, Regan W, Geng B, Alemán B, Kessler B M, Wang F, Crommie M F and Zettl A 2010 High-temperature stability of suspended single-layer graphene *physica status solidi (RRL) – Rapid Research Letters* **4** 302-4
[9] Bonaccorso F, Sun Z, Hasan T and Ferrari A C 2010 Graphene photonics and optoelectronics *Nature Photonics* **4** 611
[10] Avouris P 2010 Graphene: Electronic and Photonic Properties and Devices *Nano Letters* **10** 4285-94
[11] Alaskar Y, Arafin S, Wickramaratne D, Zurbuchen M A, He L, McKay J, Lin Q, Goorsky M S, Lake R K and Wang K L 2014 Towards van der Waals Epitaxial Growth of GaAs on Si using a Graphene Buffer Layer *Advanced Functional Materials* **24** 6629-38
[12] Araki T, Uchimura S, Sakaguchi J, Nanishi Y, Fujishima T, Hsu A, Kim K K, Palacios T, Pesquera A, Centeno A and Zurutuza A 2014 Radio-frequency plasma-excited molecular

beam epitaxy growth of GaN on graphene/Si(100) substrates *Applied Physics Express* **7** 071001
[13] Kim J, Bayram C, Park H, Cheng C-W, Dimitrakopoulos C, Ott J A, Reuter K B, Bedell S W and Sadana D K 2014 Principle of direct van der Waals epitaxy of single-crystalline films on epitaxial graphene *Nature Communications* **5** 4836
[14] Liudi Mulyo A, Konno Y, Nilsen J S, van Helvoort A T J, Fimland B-O, Weman H and Kishino K 2017 Growth study of self-assembled GaN nanocolumns on silica glass by plasma assisted molecular beam epitaxy *J. Cryst. Growth* **480** 67-73
[15] Kishino K and Ishizawa S 2015 Selective-area growth of GaN nanocolumns on Si(111) substrates for application to nanocolumn emitters with systematic analysis of dislocation filtering effect of nanocolumns *Nanotechnology* **26** 225602
[16] Hayashi H, Fukushima D, Tomimatsu D, Noma T, Konno Y and Kishino K 2015 Flip-chip bonding and fabrication of well-ordered nanocolumn arrays on sputter-deposited AlN/Si (111) substrate *physica status solidi (a)* **212** 992-6
[17] Yue Q, Li K, Kong F, Zhao J and Li W 2013 Analysis on the Light Extraction Efficiency of GaN-Based Nanowires Light-Emitting Diodes *IEEE J. Quantum Electron.* **49** 697-704
[18] Nakagawa S, Tabata T, Honda Y, Yamaguchi M and Amano H 2013 GaN Nanowires Grown on a Graphite Substrate by Radio Frequency Molecular Beam Epitaxy *Jpn. J. Appl. Phys.* **52** 08JE7
[19] Fernández-Garrido S, Ramsteiner M, Gao G, Galves L A, Sharma B, Corfdir P, Calabrese G, de Souza Schiaber Z, Pfüller C, Trampert A, Lopes J M J, Brandt O and Geelhaar L 2017 Molecular Beam Epitaxy of GaN Nanowires on Epitaxial Graphene *Nano Letters* **17** 5213-21
[20] Kang S, Mandal A, Chu J H, Park J-H, Kwon S-Y and Lee C-R 2015 Ultraviolet photoconductive devices with an n-GaN nanorod-graphene hybrid structure synthesized by metal-organic chemical vapor deposition *Scientific Reports* **5** 10808
[21] Kumaresan V, Largeau L, Madouri A, Glas F, Zhang H, Oehler F, Cavanna A, Babichev A, Travers L, Gogneau N, Tchernycheva M and Harmand J-C 2016 Epitaxy of GaN Nanowires on Graphene *Nano Letters* **16** 4895-902
[22] Chung K, Beak H, Tchoe Y, Oh H, Yoo H, Kim M and Yi G-C 2014 Growth and characterizations of GaN micro-rods on graphene films for flexible light emitting diodes *APL Materials* **2** 092512
[23] Heilmann M, Sarau G, Göbelt M, Latzel M, Sadhujan S, Tessarek C and Christiansen S 2015 Growth of GaN Micro- and Nanorods on Graphene-Covered Sapphire: Enabling Conductivity to Semiconductor Nanostructures on Insulating Substrates *Crystal Growth & Design* **15** 2079-86
[24] Heilmann M, Munshi A M, Sarau G, Göbelt M, Tessarek C, Fauske V T, van Helvoort A T J, Yang J, Latzel M, Hoffmann B, Conibeer G, Weman H and Christiansen S 2016 Vertically Oriented Growth of GaN Nanorods on Si Using Graphene as an Atomically Thin Buffer Layer *Nano Letters* **16** 3524-32
[25] Hayashi H, Konno Y and Kishino K 2016 Self-organization of dislocation-free, high-density, vertically aligned GaN nanocolumns involving InGaN quantum wells on graphene/SiO 2 covered with a thin AlN buffer layer *Nanotechnology* **27** 055302
[26] Li X, Cai W, An J, Kim S, Nah J, Yang D, Piner R, Velamakanni A, Jung I, Tutuc E, Banerjee S K, Colombo L and Ruoff R S 2009 Large-Area Synthesis of High-Quality and Uniform Graphene Films on Copper Foils *Science* **324** 1312
[27] Yoshiji H, Minoru K and Hiroshi Y 1988 Migration-Enhanced Epitaxy of GaAs and AlGaAs *Jpn. J. Appl. Phys.* **27** 169
[28] Sugihara D, Kikuchi A, Kusakabe K, Nakamura S, Toyoura Y, Yamada T and Kishino K 1999 2.6 μm/h High-Speed Growth of GaN by RF-Molecular Beam Epitaxy and

Improvement of Crystal Quality by Migration Enhanced Epitaxy *physica status solidi (a)* **176** 323-8
[29] Rybin M, Pereyaslavtsev A, Vasilieva T, Myasnikov V, Sokolov I, Pavlova A, Obraztsova E, Khomich A, Ralchenko V and Obraztsova E 2016 Efficient nitrogen doping of graphene by plasma treatment *Carbon* **96** 196-202
[30] Lin Y-C, Lin C-Y and Chiu P-W 2010 Controllable graphene N-doping with ammonia plasma *Appl. Phys. Lett.* **96** 133110
[31] Zeng J-J and Lin Y-J 2014 Tuning the work function of graphene by nitrogen plasma treatment with different radio-frequency powers *Appl. Phys. Lett.* **104** 233103
[32] Baker M A, Hammer P, Lenardi C, Haupt J and Gissler W 1997 Low-temperature sputter deposition and characterisation of carbon nitride films *Surface and Coatings Technology* **97** 544-51
[33] Kishino K, Kikuchi A, Sekiguchi H and Ishizawa S 2007 *InGaN/GaN nanocolumn LEDs emitting from blue to red* vol 6473: SPIE) p 64730T
[34] Zhang Y, Fu Q, Cui Y, Mu R, Jin L and Bao X 2013 Enhanced reactivity of graphene wrinkles and their function as nanosized gas inlets for reactions under graphene *Physical Chemistry Chemical Physics* **15** 19042-8
[35] Gohda Y and Tsuneyuki S 2012 Structural phase transition of graphene caused by GaN epitaxy *Appl. Phys. Lett.* **100** 053111
[36] Chen X J, Perillat-Merceroz G, Sam-Giao D, Durand C and Eymery J 2010 Homoepitaxial growth of catalyst-free GaN wires on N-polar substrates *Appl. Phys. Lett.* **97** 151909
[37] Urban A, Malindretos J, Klein-Wiele J H, Simon P and Rizzi A 2013 Ga-polar GaN nanocolumn arrays with semipolar faceted tips *New Journal of Physics* **15** 053045
[38] Banal R G, Funato M and Kawakami Y 2008 Initial nucleation of AlN grown directly on sapphire substrates by metal-organic vapor phase epitaxy *Appl. Phys. Lett.* **92** 241905
[39] Huang P Y, Ruiz-Vargas C S, van der Zande A M, Whitney W S, Levendorf M P, Kevek J W, Garg S, Alden J S, Hustedt C J, Zhu Y, Park J, McEuen P L and Muller D A 2011 Grains and grain boundaries in single-layer graphene atomic patchwork quilts *Nature* **469** 389-92
[40] Nakada K and Ishii A 2011 Migration of adatom adsorption on graphene using DFT calculation *Solid State Commun.* **151** 13-6
[41] Iliopoulos E and Moustakas T D 2002 Growth kinetics of AlGaN films by plasma-assisted molecular-beam epitaxy *Appl. Phys. Lett.* **81** 295-7
[42] Al Balushi Z Y, Miyagi T, Lin Y-C, Wang K, Calderin L, Bhimanapati G, Redwing J M and Robinson J A 2015 The impact of graphene properties on GaN and AlN nucleation *Surf Sci.* **634** 81-8
[43] Tabata A, Enderlein R, Leite J R, da Silva S W, Galzerani J C, Schikora D, Kloidt M and Lischka K 1996 Comparative Raman studies of cubic and hexagonal GaN epitaxial layers *J. Appl. Phys.* **79** 4137-40
[44] Sekine T, Suzuki S, Kuroe H, Tada M, Kikuchi A and Kishino K 2006 Raman Scattering in GaN Nanocolumns and GaN/AlN Multiple Quantum Disk Nanocolumns *e-Journal of Surface Science and Nanotechnology* **4** 227-32
[45] Sekine T, Komatsu Y, Iwaya R, Kuroe H, Kikuchi A and Kishino K 2017 Surface Phonons Studied by Raman Scattering in GaN Nanostructures *J. Phys. Soc. Jpn.* **86** 074602
[46] Bülbül M M, Smith S R P, Obradovic B, Cheng T S and Foxon C T 2000 Raman spectroscopy of optical phonons as a probe of GaN epitaxial layer structural quality *The European Physical Journal B - Condensed Matter and Complex Systems* **14** 423-9

[47] Kisielowski C, Krüger J, Ruvimov S, Suski T, Ager J W, Jones E, Liliental-Weber Z, Rubin M, Weber E R, Bremser M D and Davis R F 1996 Strain-related phenomena in GaN thin films *Physical Review B* **54** 17745-53
[48] McNeil L E, Grimsditch M and French R H 1993 Vibrational Spectroscopy of Aluminum Nitride *J. Am. Ceram. Soc.* **76** 1132-6
[49] Malard L M, Pimenta M A, Dresselhaus G and Dresselhaus M S 2009 Raman spectroscopy in graphene *Physics Reports* **473** 51-87
[50] Wei D, Liu Y, Wang Y, Zhang H, Huang L and Yu G 2009 Synthesis of N-Doped Graphene by Chemical Vapor Deposition and Its Electrical Properties *Nano Letters* **9** 1752-8
[51] Schiros T, Nordlund D, Pálová L, Prezzi D, Zhao L, Kim K S, Wurstbauer U, Gutiérrez C, Delongchamp D, Jaye C, Fischer D, Ogasawara H, Pettersson L G M, Reichman D R, Kim P, Hybertsen M S and Pasupathy A N 2012 Connecting Dopant Bond Type with Electronic Structure in N-Doped Graphene *Nano Letters* **12** 4025-31
[52] Jin Z, Yao J, Kittrell C and Tour J M 2011 Large-Scale Growth and Characterizations of Nitrogen-Doped Monolayer Graphene Sheets *ACS Nano* **5** 4112-7
[53] Wu M, Cao C and Jiang J Z 2010 Light non-metallic atom (B, N, O and F)-doped graphene: a first-principles study *Nanotechnology* **21** 505202
[54] Luo Z, Lim S, Tian Z, Shang J, Lai L, MacDonald B, Fu C, Shen Z, Yu T and Lin J 2011 Pyridinic N doped graphene: synthesis, electronic structure, and electrocatalytic property *Journal of Materials Chemistry* **21** 8038-44
[55] Liu J, Li Q, Zou Y, Qian Q, Jin Y, Li G, Jiang K and Fan S 2013 The Dependence of Graphene Raman D-band on Carrier Density *Nano Letters* **13** 6170-5
[56] Sarau G, Heilmann M, Bashouti M, Latzel M, Tessarek C and Christiansen S 2017 Efficient Nitrogen Doping of Single-Layer Graphene Accompanied by Negligible Defect Generation for Integration into Hybrid Semiconductor Heterostructures *ACS Applied Materials & Interfaces* **9** 10003-11
[57] Ni Z H, Chen W, Fan X F, Kuo J L, Yu T, Wee A T S and Shen Z X 2008 Raman spectroscopy of epitaxial graphene on a SiC substrate *Physical Review B* **77** 115416
[58] Shimada T, Sugai T, Fantini C, Souza M, Cançado L G, Jorio A, Pimenta M A, Saito R, Grüneis A, Dresselhaus G, Dresselhaus M S, Ohno Y, Mizutani T and Shinohara H 2005 Origin of the 2450cm−1 Raman bands in HOPG, single-wall and double-wall carbon nanotubes *Carbon* **43** 1049-54
[59] Reshchikov M A, Huang D, Yun F, Morkoç H, Molnar R J and Litton C W 2011 Excitons bound to structural defects in GaN *MRS Proceedings* **693**
[60] Shogo I, Taihei N, Nobuhiko S, Hyung Soo A, Masashi I, Toshiki H, Yoshio H, Masahito Y and Hiroshi A 2014 Nature of yellow luminescence band in GaN grown on Si substrate *Jpn. J. Appl. Phys.* **53** 11RC02
[61] Demchenko D O, Diallo I C and Reshchikov M A 2013 Yellow Luminescence of Gallium Nitride Generated by Carbon Defect Complexes *Phys. Rev. Lett.* **110** 087404